Poly(ionic liquid)-based engineered mixed matrix membranes for CO_2/H_2 separation

Ana R. Nabais[a], Ana P. S. Martins[b], Vítor D. Alves[c], João G. Crespo[a], Isabel M. Marrucho[d], Liliana C. Tomé[b,1*], Luísa A. Neves[a**]

[a] LAQV/REQUIMTE, Departamento de Química, Faculdade de Ciências e Tecnologia, Universidade NOVA de Lisboa, 2829-516 Caparica, Portugal.

[b] Instituto de Tecnologia Química e Biológica António Xavier, Universidade NOVA de Lisboa, 2780-157 Oeiras, Portugal.

[c] LEAF, Linking Landscape, Environment, Agriculture and Food, Instituto Superior de Agronomia, Universidade de Lisboa, Tapada da Ajuda, 1349-017 Lisboa, Portugal.

[d] Centro de Química Estrutural, Departamento de Engenharia Química, Instituto Superior Técnico, Universidade de Lisboa, Avenida Rovisco Pais, 1049-001 Lisboa, Portugal.

Corresponding authors: *liliana.tome@itqb.unl.pt, **lan11892@fct.unl.pt

[1] Present address: POLYMAT, University of the Basque Country UPV/EHU, Joxe Mari Korta Center, Avda. Tolosa 72, 20018 Donostia-San Sebastian, Spain.

Abstract

Poly(ionic liquid)s (PIL) have emerged as a class of versatile polyelectrolites, that can be used to prepare new materials able to achieve superior performances compared to conventional polymers. The combination of PILs with ionic liquids (ILs) may serve as a suitable matrix for the preparation of membranes for gas separation. In this work, mixed matrix membranes (MMMs) combining a pyrrolidinium-based PIL, an IL and three highly CO_2-selective metal organic frameworks (MOFs) were prepared. The different MOFs (MIL-53, $Cu_3(BTC)_2$ and ZIF-8) were used as fillers, aiming to maximize the membranes performance towards the purification of syngas. The influence of different MOFs and loadings (0, 10, 20 and 30 wt.%) on the thermal and mechanical stabilities of the membranes and their performance in terms of CO_2 permeability and CO_2/H_2 ideal selectivity was assessed. The compatibility between the materials was confirmed by SEM-EDS and FTIR spectroscopy. The prepared MMMs revealed to be thermally stable within the temperature range of the syngas stream, with a loss of mechanical stability upon the MOF incorporation. The increasing MOF content in the MMMs, resulted in an improvement of both CO_2 permeability and CO_2/H_2 ideal selectivity. Among the three MOFs studied, membranes based on ZIF-8 showed the highest permeabilities (up to 97.2 barrer), while membranes based on MIL-53 showed the highest improvement in selectivity (up to 13.3). Remarkably, all permeation results surpass the upper bound limit for the CO_2/H_2 separation, showing the membranes potential for the desired gas separation.

Keywords: Poly(Ionic Liquids); Hydrogen purification, Metal Organic Frameworks, Mixed Matrix Membranes.

1. Introduction

The increasing carbon dioxide (CO_2) concentration in the atmosphere has been one of the major concerns of the 21st century. Much of these CO_2 emissions are due to the burning of fossil fuels, which is one of the main sources of power generation in many countries. Despite the efforts to reduce CO_2 emissions and the continuous search for alternative sources of power generation, the combustion of fossil fuels will continue to play a major role in this area, because the energy supplied by renewable sources is still not sufficient to meet the current energy demands. Therefore, it is imperative to develop new and more cost-effective solutions concerning the capture and storage (CCS) of CO_2 [1].

The removal of CO_2 from pre and post combustion gas streams has been one of the main goals of the CCS technology. Over the past decades, different methods for CO_2 separation from various gas mixture streams have been investigated, such as chemical and physical absorption, adsorption, cryogenic distillation and membranes [2]. Nowadays, membrane technology is considered a very promising alternative to the conventional methods used to separate/purify gas streams. In the past years, gas separation through membranes has been deeply studied for the removal of CO_2 from flue gas streams (CO_2/N_2) [3,4], natural gas/biogas streams (CO_2/CH_4) [5,6] and fuel gas or syngas (CO_2/H_2) [7,8]. The latter is particularly interesting since it not only involves the separation of CO_2 from the gas mixture, but also allows the purification of H_2 that can be used as a clean energy source.

However, one of the major challenges concerning membranes for CO_2/H_2 separation is the development of highly permeable and selective materials that can also combine superior thermal and mechanical stabilities [9].

Poly(ionic liquid)s (PILs), are a type of polyelectrolites, prepared from polymerizable ionic liquid monomers. PILs are considered a new class of versatile functional materials that combine the chemical tunability and high CO_2 selectivity of ionic liquids (ILs) with the intrinsic macromolecular properties of polymers [10]. Ionic liquid-based membranes have already demonstrated the potential to outperform the conventional materials available for gas separation membranes, indicating its potential to be used in industrial applications [11–15].

The major advantage of using a PIL instead of an IL is the enhanced mechanical stability and improved processability, over the corresponding IL species. Despite the fact that PILs can provide a new platform to design IL-based materials for CO_2 separation, the low gas permeability and diffusivity through the solid polymer matrix achieved with neat PIL membranes led to the development of PIL/IL composite membranes, which combine the best functionalities of both materials, resulting in enhanced CO_2 transport properties [11,16–18]. Much attention has been given to the chemical compatibility of both materials, so that free-standing homogeneous composite membranes could be prepared and, its performance towards CO_2 separation maximized [11].

Other strategies can also be used to improve the CO_2 separation performance of PIL/IL membranes including the incorporation of nanofillers, such as metal organic frameworks (MOFs). These compounds are a class of porous organic-inorganic materials composed by a network of metal ions clusters linked to organic ligands [9]. The selection of the most proper linker-metal ion pair enables the tunability of these materials in terms of cavity size, surface area and chemical nature, in order to achieve specific properties towards the desired

application [19]. These unique properties distinguish MOFs from other types of porous fillers, such as zeolites, aerogels and carbon-based materials [20–22].

Incorporation of porous nanofillers into PIL/IL composite membranes has been recently studied and their potential towards CO_2 separation was reported, with promising results concerning the membranes separation performance. Hao et al. [23] prepared a series of three-component mixed matrix membranes (MMMs), consisting of a vinyl-based PIL [vbim][Tf_2N], free ILs [C_2mim][BF_4], [C_2mim][Tf_2N] and [C_2mim][$B(CN)_4$] and ZIF-8 nanoparticles, for CO_2/N_2 and CO_2/CH_4 separation. The authors concluded that all membranes exhibited an increase in CO_2 permeability, with minimal variations in the gas pair selectivity. Hudiono and co-workers [24] studied the effect of the zeolite SAPO-34 loading (up to 40 wt.%) on the CO_2/N_2 and CO_2/CH_4 separation performance using MMMs, comprising a styrene-based or vynil-based PIL and IL [C_2mim][Tf_2N]. The obtained results showed that the addition of zeolite particles increased the CO_2 permeability and selectivity of the MMMs, as long as there was an adequate amount of IL, to coat the surface of the SAPO-34 particles and compatibilize them with the polymeric matrix. The authors also observed that the increase on IL content and fixed SAPO-34 concentration (20 wt.%), resulted in an overall improvement of gas permeability due to a higher diffusivity through the polymeric matrix. More recently, in an attempt to determine and optimize the factors affecting CO_2/CH_4 separation performance in PIL/IL/zeolite MMMs, Singh et al. [25] produced membranes combining a cross-linked PIL, an IL and zeolite particles. The authors reported MMMs with CO_2/CH_4 separation performances above the 2008 Robeson upper bound limit [26].

Bearing in mind the encouraging results mentioned above for PIL/IL/Inorganic filler MMMs, this work reports the preparation and characterization of a new group of MMMs, comprising a pyrrolidinium-based PIL, poly(diallylmethylammonium)bis(trifluoromethylsulfonyl) imide, poly[Pyr_{11}][Tf_2N], an IL comprising the same structural anion, 1-butyl-3-methylpyrrolidinium bis(trifluoromethylsulfonyl) imide, [C_4mpyr][Tf_2N], with three different MOFs (MIL-53, $Cu_3(BTC)_2$ and ZIF-8), which have been reported to present high potential for CO_2 adsorption [27–29]. Pyrrolidinium-based PILs have proven to be a suitable polymeric matrix for CO_2 separation membranes. Moreover, the synthetic route used for pyrrolidinium-based PILs is straightforward: A simple metathesis reaction is performed using a commercially available polyelectrolite, without need of synthetic and purification steps at the monomer level, as required for imidazolium-based PILs [16,17]. It is expected that the incorporation of highly CO_2-selective MOFs into composite membranes with structurally similar PIL and IL, will induce higher CO_2 separation performances. Gas permeation experiments were performed for pure CO_2 and H_2 and the membranes' separation performance was assessed. Also, membranes characterization was performed by Fourier Transform Infrared spectroscopy (FTIR), Scanning Electron Microscopy with Energy Dispersive Spectroscopy (SEM-EDS), Thermogravimetric Analysis (TGA) and mechanical properties through puncture tests.

2. EXPERIMENTAL

2.1. Materials

Poly[Pyr_{11}][Tf_2N], previously sinthesized [30], and [C_4mpyr][Tf_2N], supplied by Iolitec (Germany) with a mass fraction purity of 99%, were used as PIL and IL, respectively, to prepare the membranes. MIL-53(Al), $Cu_3(BTC)_2$ and ZIF-8 were synthesized by BASF SE (Germany) and supplied by Sigma Aldrich (Portugal), as Basolite™ A100, Basolite™ C300 and Basolite™ Z1200, respectively. Dimethylformamide (DMF) was suplied by Sigma Aldrich (Portugal) and used as solvent. Carbon dioxide, CO_2 (high purity grade, 99.998%) and hydrogen, H_2 (purity grade > 99.99%) gases were supplied by Praxair (Portugal). Table 1 provides a description of the MOFs characteristics used in this work.

Table 1. Characteristics of MOFs used in this work.

MOF	Chemical formula	Cavity diameter (Å)	Particle size (μm)	Porous volume (cm^3g^{-1})	BET surface area (m^2g^{-1})	Refs.
MIL-53	$C_{24}H_{12}Al_2O_{12}$	9	0.2	0.30	1100-1300	[27,31,32]
$Cu_3(BTC)_2$	$C_{18}H_6Cu_3O_{12}$	9	10	0.50	1300-1800	[27,32,33]
ZIF-8	$C_8H_{10}N_4Zn$	11	0.3	0.62	1500-1700	[27,32,34]

2.2. Preparation of PIL-based mixed matrix membranes

PIL/IL composite membrane and PIL/IL/MOF MMMs with different MOF concentrations (10, 20 and 30 wt.%) were prepared through the solvent evaporation method. Initially, 0.6 g of poly[Pyr_{11}][Tf_2N] and 0.4 g of

160 [C_4mpyr][Tf_2N] were dissolved in 8 mL of DMF. The resulting solution was then
161 magnetically stirred for 8 hours (MIX 15 eco, 2mag). Simultaneously, the
162 additive solutions were prepared in separate vials, by dissolving 0.1 g (10
163 wt.%), 0.2 g (20 wt.%) or 0.3 g (30 wt.%) of MOF in 8 mL of DMF. These
164 solutions were then sonicated in an ultrasound bath for 4 hours and then stirred
165 for the same period. Afterwards, the solutions were mixed and left stirring
166 overnight. Finally, membrane solutions were casted in Teflon plates and heated
167 over a period of 7-8 hours at a constant temperature of 343 K.
168
169 **2.3. Characterization of membranes**
170 2.3.1. Fourier Transform Infrared spectroscopy (FTIR) analysis
171 The FTIR analysis was performed in order to confirm the incorporation of both
172 IL and MOFs in the membranes and also to determine the interactions
173 established between the materials in the membrane. The FTIR spectra of the
174 pure PIL, IL, MOFs and the prepared MMMs were acquired using a Perkin
175 Elmer Spectrum two spectrometer. All spectra were collected using 10 scans,
176 from 400 to 4000 cm^{-1}.
177
178 2.3.2. Scanning Electron Microscopy with Energy Dispersive
179 Spectroscopy (SEM-EDS)
180 The distribution of the MOF in the PIL/IL matrix, as well as the compatibility
181 between the MOF, IL and PIL phase in the MMMs were investigated through
182 Scanning Electron Microscopy equipped with Energy Dispersive Spectroscopy
183 (SEM-EDS). The SEM-EDS images were acquired using a JEOL 7001F
184 scanning electron microscope (FEG-SEM, JEOL, USA Inc.) equipped with a

185 field emission gun operated at 15 kV. All tested samples were coated with a thin
186 Pd/Au layer.
187
188 2.3.3. Thermogravimetric Analysis (TGA)
189 The thermal stabilities of the PIL, IL, MOFs, and all prepared MMMs were
190 evaluated by thermogravimetric analysis (TGA), using a TA Instrument Model
191 TGA Q50. The pure MOFs, PIL, IL, PIL/IL composite membrane and prepared
192 MMMs were heated from ambient temperature to 1073 K, at a heating rate of 10
193 K min^{-1}. All the experiments were carried out under a constant nitrogen flow of
194 40 mL min^{-1}. The obtained data was analysed using a Universal Analysis 4.5A
195 software.
196
197 2.3.4. Mechanical Properties
198 The normalized puncture strength and elongation at break of the MMMs were
199 evaluated through puncture tests, using a TA XT Plus texture analyser (Stable
200 Micro Systems, UK). The prepared membranes were punctured through a hole
201 with a cylindrical probe of 2 mm diameter, at a constant speed rate of 1 mm s^{-1}.
202 For each membrane, at least three replicates were made and the mean value of
203 the obtained normalized puncture strength and elongation at break was
204 determined. The puncture strength was calculated according to the following
205 equation

$$\sigma = \frac{F}{A}, (1)$$

206 where σ is the puncture strength (Pa), F is the force exerted by the probe (N)
207 and A is the probe area (m^2). To more accurately compare the experimental

208 results, the puncture strength was normalized so the membrane thickness
209 would not influence the obtained results, according to the equation

$$\sigma_n = \frac{\sigma}{l}, (2)$$

210 where σ_n is the normalized puncture strength (MPa mm^{-1}) and *l* is the
211 membrane thickness (mm).
212
213 2.3.5. Pure Gas Permeation experiments
214 Single gas CO_2 and H_2 permeabilities and CO_2/H_2 ideal selectivity were
215 determined using a gas permeation setup described elsewhere [15]. The
216 system is composed by a stainless steel cell with a feed and permeate
217 compartments, separated by the membrane. To ensure a constant temperature
218 during the experiments, the permeation cell was placed in a thermostatic water
219 bath (Julabo GmBH ED, Germany), where the temperature was set at 303 K. All
220 experiments started by pressurizing each compartment with CO_2 or H_2, and,
221 after the pressure was stabilized, a transmembrane driving force of about 0.7
222 bar was established. The pressure variation over time, in each compartment,
223 was measured by pressure transducers (Druck PCDR 910, 99166 and 991675,
224 UK). The pressure monitoring and data acquisition were controlled by an in-
225 house developed software. The permeability of each pure gas through each
226 membrane was calculated according to:

$$\frac{1}{\beta}\ln\frac{P_{feed_0} - P_{perm_0}}{P_{feed} - P_{perm}} = \frac{1}{\beta}\ln\frac{\Delta P_0}{\Delta P} = P\frac{t}{l}, \qquad (3)$$

227 where p_{feed} and p_{perm} are the pressures (bar) in the feed and permeate sides,
228 respectively, *P* is the membrane permeability (m^2 s^{-1}), *t* is the time (s), and *l* is

229 the membrane thickness (m) [35]. β (m^{-1}) is dependent of the cell geometry, and
230 is given by the following equation:

$$\beta = A\left(\frac{1}{V_{feed}} + \frac{1}{V_{perm}}\right), (4)$$

231 where A is the membrane area (m^2) and V_{feed} and V_{perm} represent the
232 volumes (m^3) of the feed and permeate compartments, respectively. The pure
233 gas permeability can be determined by ploting $1/\beta\ ln(\Delta P_0/\Delta P)$ as a function of
234 t/l. The ideal selectivity was calculated by dividing the permeability of the more
235 permeable specie (CO_2) by the permeability of the least permeable specie (H_2),
236 according to:

$$\alpha_{CO_2/H_2} = \frac{P_{CO_2}}{P_{H_2}}, (5)$$

237

238 **3. RESULTS AND DISCUSSION**

239 **3.1. FTIR analysis**

240 The interactions established between materials in the MMMs were studied by
241 FTIR spectroscopy. MMMs with 30 wt.% MOF loading were analysed, in order
242 to have a sufficient concentration of MOF for the equipment to clearly detect it.
243 The FTIR spectra of the PIL/IL composite membrane, MOFs and respective
244 MMMs are depicted in Figure 1. In the PIL/IL membrane spectrum, the bands
245 between 3030 cm^{-1} and 2860 cm^{-1} and the band at around 1473 cm^{-1} are
246 attributed to the CH2 stretching vibrations and CH3 bending vibrations
247 originating from the methyl units of the cationic backbone, respectively. Bands
248 at 1347 cm^{-1}, 1175 cm^{-1}, 1132 cm^{-1} and 1050 cm^{-1} are attributed to the Tf_2N
249 anion [16].

The obtained IR patterns of the MOFs studied are similar to those found in literature. For MIL-53, the peaks at 1577 cm^{-1} and 1508 cm^{-1}, are characteristic of carboxylate groups which are coordinated to Al. More specifically, these peaks are attributed to the asymmetric CO_2 stretching mode of carboxylic groups. The peak observed at 1417 cm^{-1} corresponds to the CO_2 symmetric stretching vibration [31,36].

For $Cu_3(BTC)_2$, the region between 1650 cm^{-1} and 1150 cm^{-1} corresponds to bands associated with carboxylate groups of the BTC ligand. The region below 1150 cm^{-1} is where most vibrational modes of the BTC ligand are detected. The peak at 1110 cm^{-1} and the peaks at 758 cm^{-1} and 729 cm^{-1} correspond to the in-plane and out-of-plane C-H bending modes, respectively, all associated with the aromatic ring of the BTC ligand [37].

The ZIF-8 spectrum shows a small peak at 3000 cm^{-1}, possibly due to the C-H stretching vibrational mode of the methyl group present in the linker. The peak at 1584 cm^{-1} corresponds to the C=N bond stretch modes, while the peaks at 1447 cm^{-1} and 1383 cm^{-1} correspond to the entire ring stretch. The region between 1311 cm^{-1} and 995 cm^{-1} is attributed to an in-plane bending of the ring, while the region between 759 cm^{-1} and 685 cm^{-1} corresponds to the aromatic sp^2 C-H bending. The peak observed at 421 cm^{-1} is characteristic of the metal Zn [34].

The MMMs with 30 wt.% MIL-53 and $Cu_3(BTC)_2$, present peak location shifts to lower wavenumbers, compared to the PIL/IL membrane spectrum (1672 cm^{-1} to 1600 cm^{-1} and 1672 cm^{-1} to 1636 cm^{-1}, respectively), which probably corresponds to molecular interactions between the MOF and the PIL/IL. Peak location shifts to lower wavenumbers usually results from the formation of

hydrogen bonds between molecules, such as the MOF particles and the PIL/IL. On the other hand, the spectra of the MMM with 30 wt.% ZIF-8 does not present any peak location shift, suggesting that no strong chemical interaction occurs between the components, as also observed in previous works [34]. This may be due to the chemical nature of ZIF-8, which prevents the MOF from forming polar/hydrogen bonds with other materials [38,39].

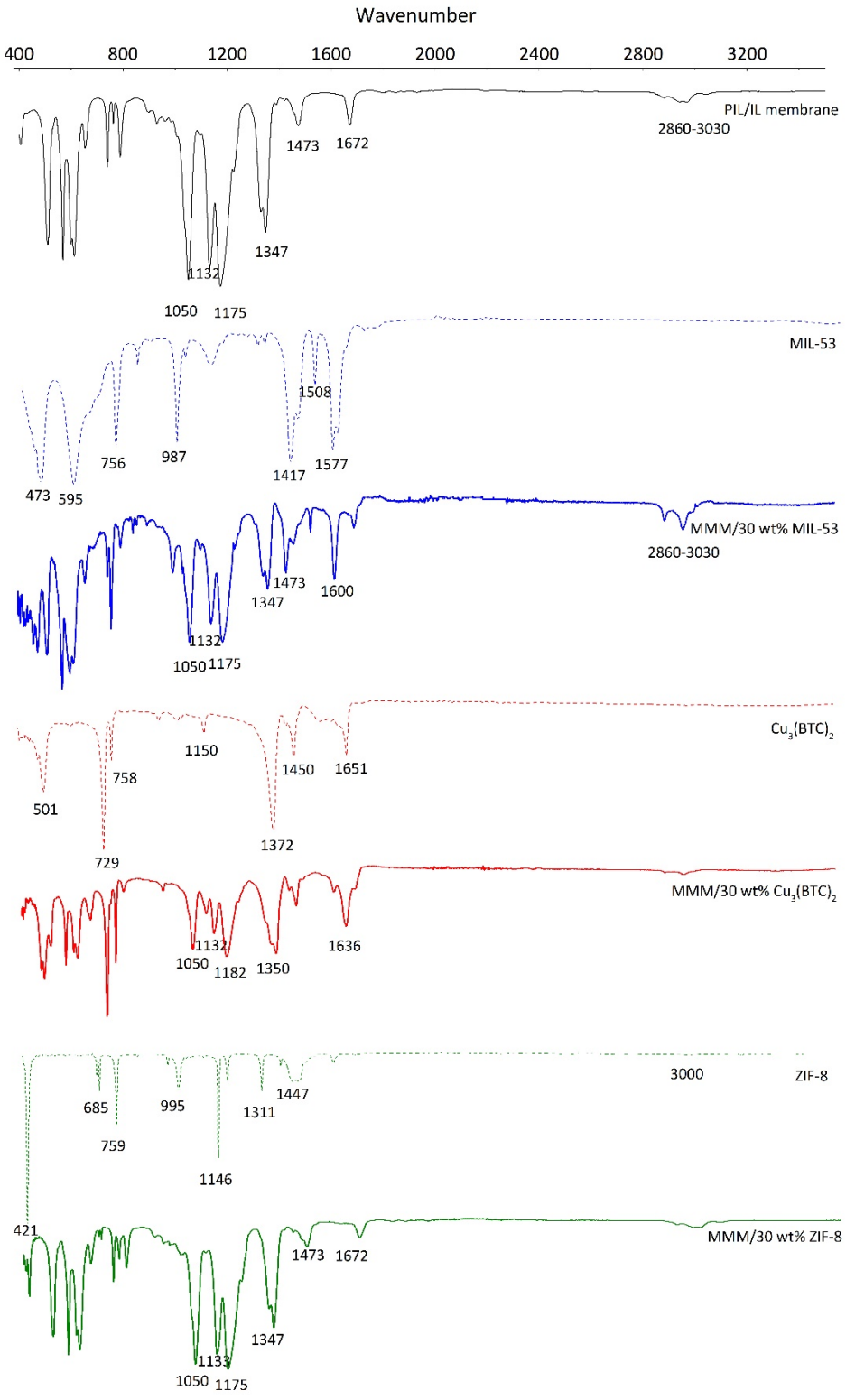

Figure 1. FTIR spectra of the PIL/IL membrane, MOFs and respective MMMs with 10 20 and 30 wt% MOF loading.

3.2. SEM-EDS

Figure 2 (a-f) shows the obtained cross-section (a, c, e) and SEM-EDS images (b, d, f) of the prepared MMMs with 30 wt.% MIL-53 (a, b), $Cu_3(BTC)_2$ (c, d) and ZIF-8 (e, f). SEM-EDS images show the distribution of the MOF particles in the membrane surface, by identifying the metal element present in the MOF: Al in MIL-53 (blue), Cu in $Cu_3(BTC)_2$ (red) and Zn in ZIF-8 (green). It can be seen that dense PIL/IL membranes with an homogeneous MOF dispersion throughout the membrane surface were achieved, indicating a good interaction between the MOF particles and the PIL/IL composite matrix, without significant particles agglomerates or visible deformations. Although only MMMs with 30 wt.% MOF loading are presented in Figure 2, a dense morphology with a good MOF dispersion was achieved for all the prepared MMMs. It is important to note that a homogeneous MOF dispersion in the PIL/IL membrane is essential to obtain high gas separation performances, especially in terms of selectivity.

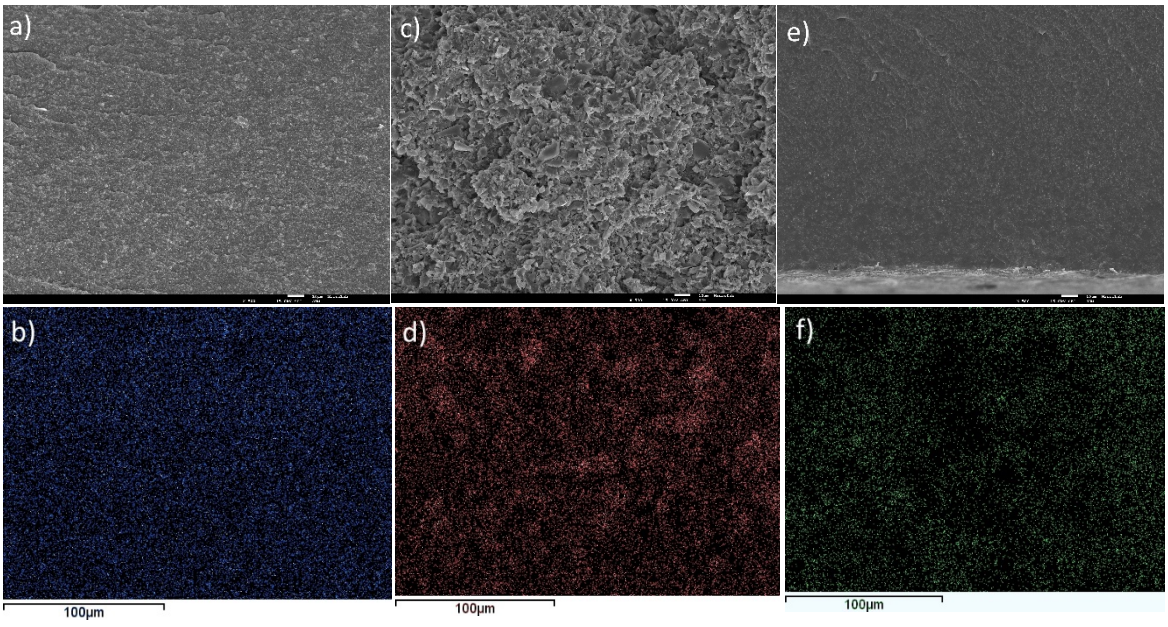

Figure 2. Cross-section (a, c, e) and surface (b, d, f) images of the prepared MMMs with 30 wt% MIL-53 (a, b), Cu3(BTC)2 (c, d) and ZIF-8 (e, f), respectively. The colors blue, red and green represent the distribution of the metal present in MIL-53 (Al), Cu3(BTC)2 (Cu) and ZIF-8, respectively.

3.3. Mechanical Properties

Table 2 shows the mechanical properties of the PIL/IL composite membrane and MMMs with 10, 20 and 30 wt.% MOF. The normalized puncture strength for MMMs with 20 and 30 wt.% of $Cu_3(BTC)_2$ and ZIF-8 is lower when compared to the PIL/IL composite membrane. This can be a result of the lower free volume available. Due to the presence of inorganic particles, the polymer chains have lower mobility within the composite membrane, which also explains the decrease of their elongation/flexibility properties. On top of that, this effect can also be attributed to randomly distributed filler agglomerates in the MMMs, that can act as stress concentrators and reduce the strength of the membrane, even though these agglomerates were not detected in the SEM analysis. This is in agreement with what has been discussed and reported in previous works [27].

Conversely, increasing the content of MIL-53 in the PIL/IL material promoted a continuous increase in the puncture strength. This means that the chemical nature of the MIL-53 is more compatible with the PIL/IL matrix, suggesting that stronger interactions between MOF particles, PIL and IL may be probably formed.

318 **Table 2.** Normalized puncture strength and elongation at break of the prepared PIL/IL
319 composite membrane and MMMs with 10, 20 and 30 wt% MOF loading.

MOF	MOF loading (%)	Normalized puncture strength (MPa mm^{-1})	Elongation at break (%)
-	0	1.03±0.05	20.16±1.16
	10	2.23±0.19	9.05±0.20
MIL-53	20	2.30±0.10	6.45±0.17
	30	3.24±0.06	3.75±0.47
	10	0.93±0.03	6.01±0.78
$Cu_3(BTC)_2$	20	0.66±0.04	4.05±0.35
	30	0.59±0.04	1.79±0.64
	10	1.45±0.10	8.57±0.70
ZIF-8	20	0.73±0.03	4.51±0.34
	30	0.37±0.01	1.85±0.13

320

321 ### 3.4. Thermogravimetric analysis

322 Figure 3 shows the TGA profiles of the prepared PIL/IL composite membrane,
323 pure MOFs and respective MMMs. The obtained TGA profiles of the MOFs
324 used in this work are very similar to those reported in the literature [27,32,33]. In
325 general, the prepared MMMs show a weight loss stage when the temperature is
326 raised to 473 K, possibly due to evaporation of some residual solvent, except
327 for MMMs with ZIF-8. All the MMMs show similar behaviour to that of the
328 composite membrane until around 573 K. The thermal decomposition (T_d) of the
329 PIL/IL membrane starts around 654 K. It has been observed that the T_d
330 decreases with increasing MOF loading, down to 639 K, 598 K and 615 K for
331 the MMMs with 30 wt.% loading of MIL-53, $Cu_3(BTC)_2$ and ZIF-8, respectively.
332 Above this temperatures it is possible to see a continuous weight loss, which

consequently results in a complete degradation of the membrane. Similar results for MOF-containing MMMs have been obtained in previous works [40,41].

Since syngas streams temperature ranges from 313-523 K [11] and no major weight losses were detected in this range of temperature, the obtained TGA results show that the proposed MMMs may be suitable for application in CO_2/H_2 gas separation.

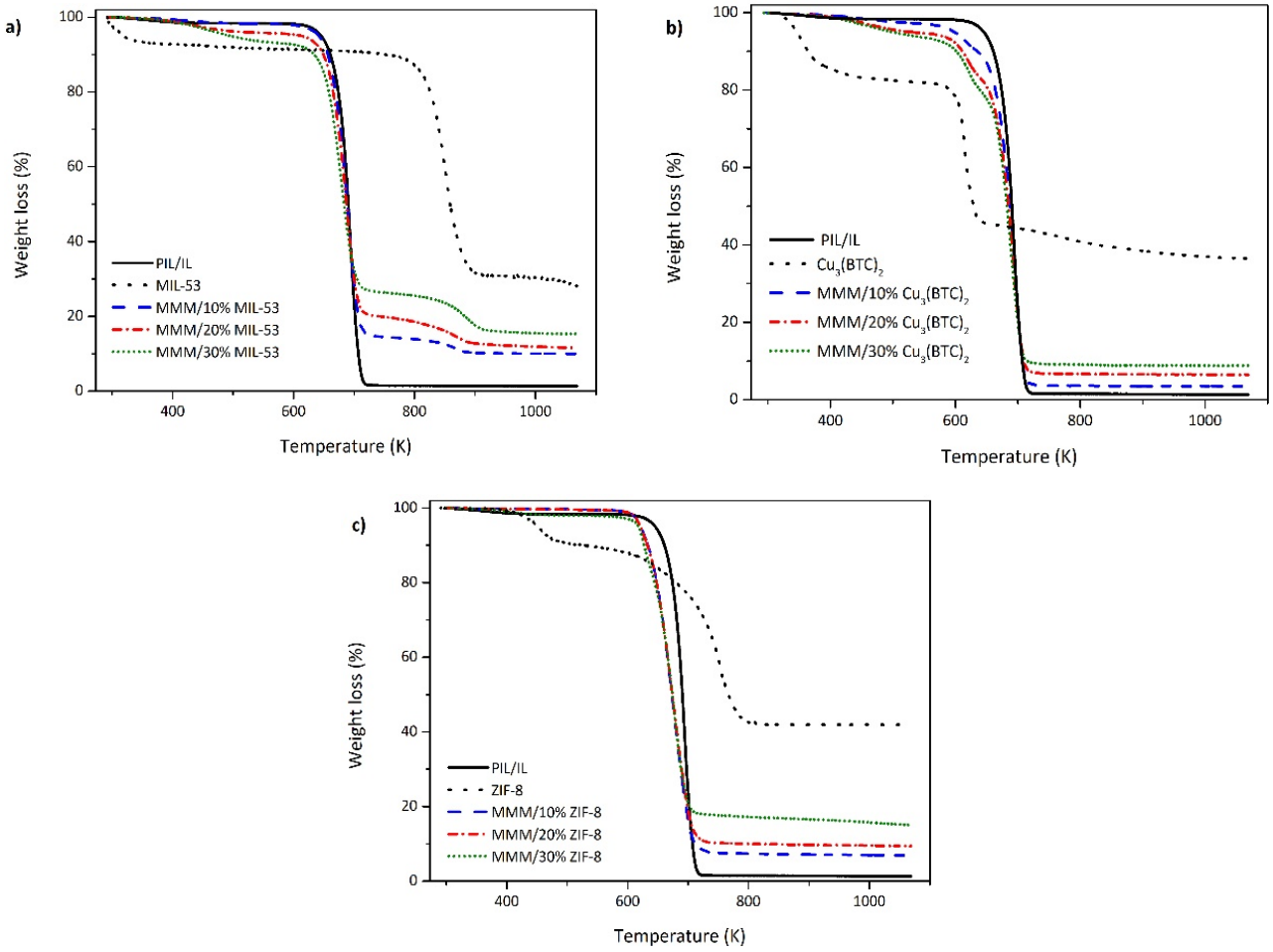

Figure 3. TGA profiles of the pure MOFs, PIL/IL composite membrane and MMMs with 10, 20 and 30 wt% MOF loading.

3.5. Pure gas permeation experiments

The measured single gas permeability and CO_2/H_2 ideal selectivity of the PIL/IL composite membrane and MMMs, are shown in Figure 4 and Figure 5, respectively. For a 10 wt.% MOF incorporation, MMMs with $Cu_3(BTC)_2$ and ZIF-8 show lower CO_2 permeabilities, compared to the PIL/IL composite membrane probably due to an increase in tortuosity caused by the low concentration of MOF particles, as they may restrain the diffusion of gases through the membrane [42,43]. Nevertheless, with a continuous increase in MOF loading this obstacle was surpassed, which resulted in increased CO_2 permeabilities, surpassing the obtained value for the PIL/IL composite membrane, with the highest permeability value here obtained for the 30 wt.% loading MMMs.

Unlike many reported results for CO_2 and H_2 permeability in membranes made with more conventional polymers [34,44,45], in this work we observed that CO_2 permeability is much higher than that of H_2. The H_2 permeability also increases with increasing MOF loading, but this increase is not as significant as it is for CO_2. Even though H_2 has a lower kinetic diameter (2.9 Å) compared with CO_2 (3.3 Å), the condensability, the high ionic content of the PIL and IL, and the interactions between CO_2 and the membrane materials, improved the CO_2 permeability, since this gas is much more soluble in the membrane, compared to H_2 [46,47].

In fact, due to the favoured CO_2 permeability, a continuous increase in the CO_2/H_2 ideal selectivity with increasing MOF loading can be observed in Figure 5, surpassing the obtained result for the PIL/IL composite membrane. This happens probably due to the occurrence of specific interactions between the CO_2 and the MOF frameworks, due to the high CO_2 adsorption capacity of

these materials. This leads to a preferential CO_2 adsorption that ensures a discrimination between the gas molecules, improving the selectivity of these MMMs [27].

Attention should also be given to the influence of the MOF type. The role of the MOFs in the membranes separation performances can be differentiated based on their porous volume, cavity topology and BET surface area (Table 1). From Figure 4, it can be observed that, overall, the CO_2 permeability increases in order MMM/MIL-53<MMM/$Cu_3(BTC)_2$<MMM/ZIF-8. This trend may be related to the higher porous volume of ZIF-8 and BET surface area as it can be seen in Table 1, compared to that of $Cu_3(BTC)_2$ [27,32]. This confirms that CO_2 permeability is influenced not only by the adsorption properties and solubility coefficient, but also by the diffusion coefficient, namely the cavity size and the porous volume of the MOF in the membrane.

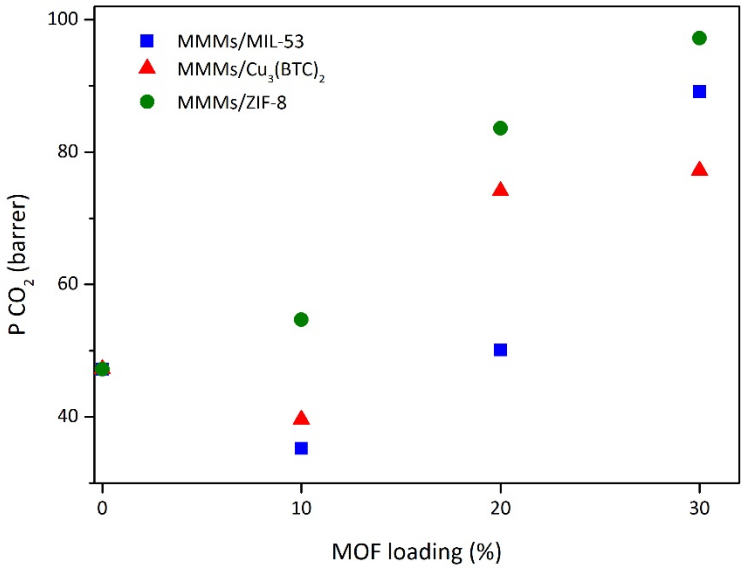

Figure 4. Single-gas CO_2 permeability of the prepared PIL/IL composite membrane and MMMs with 10, 20 and 30 wt% MOF loading.

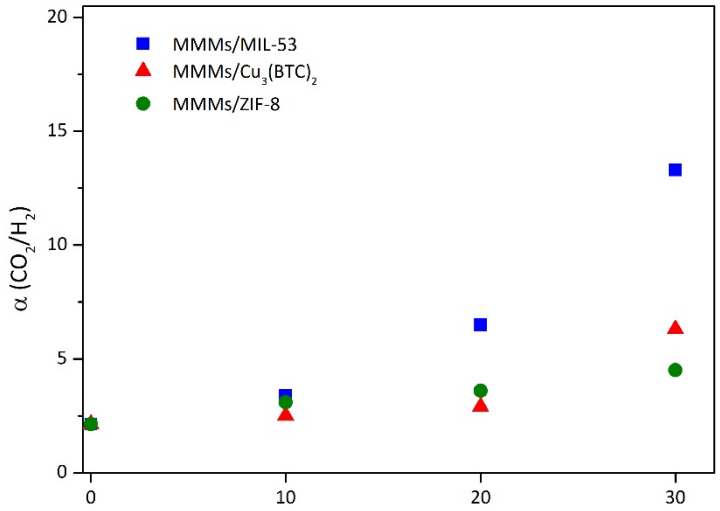

Figure 5. CO_2/H_2 ideal selectivity of the prepared PIL/IL composite membrane and MMMs with 10, 20 and 30 wt% MOF loading.

In order to more accurately evaluate the overall MMMs performance, the upper bound correlation for CO_2/H_2 separation is represented in Figure 6. These upper bound limits were first studied by Robeson et al. [26], for the H_2/CO_2 separation based on data obtained from measurements performed at low temperatures, where the results showed that the permeability of H_2 was much higher than that of CO_2. Later, different works showed that, depending on the membrane materials and their interactions with the gas molecules, it is also possible to obtain a higher CO_2 permeability compared to H_2. This led to the development of a new by Rowe et al. [48] , from which resulted the upper bound relation seen in Figure 6. Regarding the CO_2/H_2 separation, it is observed that not only all results obtained in this work are above the upper bound limit, but also a clear improvement over the PIL/IL composite membrane was achieved. These results show that the incorporation of CO_2-selective MOFs in the membrane offers clear advantages and can be considered a viable option in CO_2/H_2 separation.

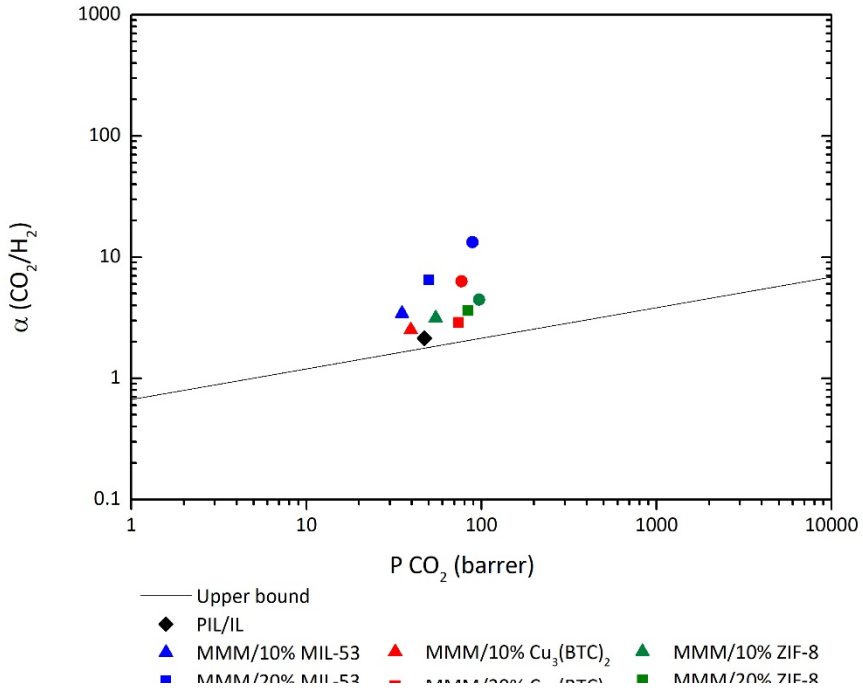

Figure 6. CO_2/H_2 MMMs ideal selectivity as a function of CO_2 permeability.

4. CONCLUSIONS

In this work, poly(ionic liquid)-based mixed matrix membranes (MMMs) were prepared, with a pyrrolidinium-based PIL and an IL containing the same structural anion, $[Tf_2N]$, serving as a composite matrix. The influence of different MOF incorporation degrees on the MMMs gas separation performance as well as on their thermal and mechanical stabilities was evaluated. The obtained MMMs were also analyzed by SEM-EDS and FTIR spectroscopy, to confirm the successful incorporation of both IL and MOF particles in the membrane, which resulted in a homogeneous and defect-free structure. Thermally stable MMMs, within the temperature range of the syngas stream, were obtained.

According to the results of the pure gas permeation experiments, an improvement in both CO_2 permeability and CO_2/H_2 ideal selectivity was achieved. These results were mainly attributed to the high ionic content of the PIL/IL composite matrix and the high CO_2 adsorption properties of the MOFs.

Also, the membranes permeability was considerably influenced by the intrinsic characteristics of the incorporated MOFs, namely their porous volume, cavity topology and BET surface area. Among the three different types of MMMs, membranes based on MIL-53 showed the highest improvement in ideal selectivity (up to 13.3), while membranes based on ZIF-8 achieved the highest results for CO_2 permeability, up to 97.2 barrer with 30 wt.% loading.

Moreover, the prepared membranes were able to surpass the CO_2/H_2 upper bound limit, due to the simultaneous improvement in permeability and selectivity. The above mentioned results may be an indicator of the potential of the prepared membranes for the CO_2/H_2 separation from syngas streams, and also of the advantage of incorporating CO_2-selective MOFs to induce higher separation performances.

Future work will be focused on gas permeation experiments at experimental conditions that mimic those of a real syngas stream, in terms of gas composition, pressure and temperature. Furthermore, the effect of water vapor in the membranes separation performance will also be assessed.

ACKNOWLEDGEMENTS

This work was partially supported by R&D Units UID/Multi/04551/2013 (Green-it), UID/QUI/00100/2013 (CQE), and the Associated Laboratory Research Unit for Green Chemistry, Technologies and Clean Processes, LAQV which is financed by national funds from FCT/MCTES(UID/QUI/50006/2013) and co-financed by the ERDF under the PT2020 Partnership Agreement (POCI-01-0145-FEDER-007265). Ana R. Nabais, Luísa A. Neves and Liliana C. Tomé acknowledge FCT/MCTES for financial support through project PTDC/CTM-

POL/2676/2014, FCT Investigator Contract IF/00505/2014 and Post-doctoral research grant SFRH/BDP/101793/2014, respectively. This project has received funding from the European Union's Horizon 2020 research and innovation programme under the Marie Sklodowska-Curie grant agreement No 745734.

REFERENCES

[1] S.M. Benson, F.M. Orr, Carbon dioxide capture and storage, MRS Bull. 33 (2008) 303–305. doi:10.1557/mrs2008.63.

[2] D.M.D. Alessandro, B. Smit, J.R. Long, Carbon Dioxide Capture Carbon Dioxide Capture : Prospects for New Materials Angewandte, Angew. Chem. Int. Ed. 49 (2010) 6058–6082. doi:10.1002/anie.201000431.

[3] C.E. Powell, G.G. Qiao, Polymeric CO2/N2 gas separation membranes for the capture of carbon dioxide from power plant flue gases, J. Membr. Sci. 279 (2006) 1–49. doi:10.1016/j.memsci.2005.12.062.

[4] L. Zhao, E. Riensche, R. Menzer, L. Blum, D. Stolten, A parametric study of CO2/N2 gas separation membrane processes for post-combustion capture, J. Membr. Sci. 325 (2008) 284–294. doi:10.1016/j.memsci.2008.07.058.

[5] G. Valenti, A. Arcidiacono, J.A. Nieto Ruiz, Assessment of membrane plants for biogas upgrading to biomethane at zero methane emission, Biomass and Bioenergy. 85 (2016) 35–47. doi:10.1016/j.biombioe.2015.11.020.

[6] M. Scholz, T. Melin, M. Wessling, Transforming biogas into biomethane

using membrane technology, Renew. Sustain. Energy Rev. 17 (2013) 199–212. doi:10.1016/j.rser.2012.08.009.

[7] T.C. Merkel, M. Zhou, R.W. Baker, Carbon dioxide capture with membranes at an IGCC power plant, J. Membr. Sci. 389 (2012) 441–450. doi:10.1016/j.memsci.2011.11.012.

[8] D. Figueroa, T. Fout, S. Plasynski, H. Mcilvried, R.D. Srivastava, Advances in CO2 capture technology — The U.S. Department of Energy's Carbon Sequestration Program, Int. J. Greenh. Gas Control. 2 (2008) 9–20. doi:10.1016/S1750-5836(07)00094-1.

[9] E. Adatoz, A.K. Avci, S. Keskin, Opportunities and Challenges of MOF-based Membranes in Gas Separations, Sep. Purif. Technol. 152 (2015) 207–237. doi:10.1016/j.seppur.2015.08.020.

[10] Z. Dai, R.D. Noble, D.L. Gin, X. Zhang, L. Deng, Combination of ionic liquids with membrane technology: A new approach for CO2 separation, J. Membr. Sci. 497 (2016) 1–20. doi:10.1016/j.memsci.2015.08.060.

[11] L.C. Tomé, I.M. Marrucho, Ionic liquid-based materials: a platform to design engineered CO2 separation membranes, Chem. Soc. Rev. 45 (2016) 2785–2824.

[12] S. Kasahara, E. Kamio, T. Ishigami, H. Matsuyama, Effect of water in ionic liquids on CO2permeability in amino acid ionic liquid-based facilitated transport membranes, J. Membr. Sci. 415–416 (2012) 168–175. doi:10.1016/j.memsci.2012.04.049.

[13] S. Kasahara, E. Kamio, H. Matsuyama, Improvements in the CO2

permeation selectivities of amino acid ionic liquid-based facilitated transport membranes by controlling their gas absorption properties, J. Membr. Sci. 454 (2014) 155–162. doi:10.1016/j.memsci.2013.12.009.

[14] S. Uk Hong, D. Park, Y. Ko, I. Baek, Polymer-ionic liquid gels for enhanced gas transport, Chem. Commun. 1 (2009) 7227. doi:10.1039/b913746g.

[15] L.A. Neves, J.G. Crespo, I.M. Coelhoso, Gas permeation studies in supported ionic liquid membranes, J. Membr. Sci. 357 (2010) 160–170. doi:10.1016/j.memsci.2010.04.016.

[16] L.C. Tomé, M.A. Aboudzadeh, L.P.N. Rebelo, C.S.R. Freire, D. Mecerreyes, I.M. Marrucho, Polymeric ionic liquids with mixtures of counter-anions: a new straightforward strategy for designing pyrrolidinium-based CO2 separation membranes, J. Mater. Chem. A. 1 (2013) 10403–10411.

[17] L.C. Tomé, M. Isik, C.S.R. Freire, D. Mecerreyes, I.M. Marrucho, Novel pyrrolidinium-based polymeric ionic liquids with cyano counter-anions: High performance membrane materials for post-combustion CO2separation, J. Membr. Sci. 483 (2015) 155–165.

[18] L.C. Tomé, D.C. Guerreiro, R.M. Teodoro, V.D. Alves, I.M. Marrucho, Effect of polymer molecular weight on the physical properties and CO2/N2separation of pyrrolidinium-based poly(ionic liquid) membranes, J. Membr. Sci. 549 (2018) 267–274. doi:10.1016/j.memsci.2017.12.019.

[19] M. Rezakazemi, A. Ebadi Amooghin, M.M. Montazer-Rahmati, A.F.

524 Ismail, T. Matsuura, State-of-the-art membrane based CO2separation
525 using mixed matrix membranes (MMMs): An overview on current status
526 and future directions, Prog. Polym. Sci. 39 (2014) 817–861.
527 doi:10.1016/j.progpolymsci.2014.01.003.

528 [20] S.L. James, Metal-organic frameworks, Chem. Soc. Rev. 3 (2003) 276–
529 288. doi:10.1039/b200393g.

530 [21] B.S.T. Meek, J.A. Greathouse, M.D. Allendorf, Metal-Organic
531 Frameworks : A Rapidly Growing Class of Versatile Nanoporous
532 Materials, Adv. Mater. 23 (2011) 249–267. doi:10.1002/adma.201002854.

533 [22] B. Zornoza, C. Tellez, J. Coronas, J. Gascon, F. Kapteijn, Microporous
534 and Mesoporous Materials Metal organic framework based mixed matrix
535 membranes : An increasingly important field of research with a large
536 application potential, Microporous Mesoporous Mater. 166 (2013) 67–78.
537 doi:10.1016/j.micromeso.2012.03.012.

538 [23] L. Hao, P. Li, T. Yang, T.S. Chung, Room temperature ionic liquid/ZIF-8
539 mixed-matrix membranes for natural gas sweetening and post-
540 combustion CO2 capture, J. Membr. Sci. 436 (2013) 221–231.

541 [24] Y.C. Hudiono, T.K. Carlisle, A.L. LaFrate, D.L. Gin, R.D. Noble, Novel
542 mixed matrix membranes based on polymerizable room-temperature ionic
543 liquids and SAPO-34 particles to improve CO 2 separation, J. Membr. Sci.
544 370 (2011) 141–148. doi:10.1016/j.memsci.2011.01.012.

545 [25] Z. V. Singh, M.G. Cowan, W.M. McDanel, Y. Luo, R. Zhou, D.L. Gin, R.D.
546 Noble, Determination and optimization of factors affecting

547 CO2/CH4separation performance in poly(ionic liquid)-ionic liquid-zeolite
548 mixed-matrix membranes, J. Membr. Sci. 509 (2016) 149–155.
549 doi:10.1016/j.memsci.2016.02.034.

550 [26] L.M. Robeson, The upper bound revisited, J. Membr. Sci. 320 (2008)
551 390–400. doi:10.1016/j.memsci.2008.04.030.

552 [27] S. Basu, A. Cano-Odena, I.F.J. Vankelecom, MOF-containing mixed-
553 matrix membranes for CO2/CH4 and CO2/N2 binary gas mixture
554 separations, Sep. Purif. Technol. 81 (2011) 31–40.
555 doi:10.1016/j.seppur.2011.06.037.

556 [28] L. Zhu, H. Yu, H. Zhang, J. Shen, L. Xue, C. Gao, B. Van Der Bruggen,
557 Mixed matrix membranes containing MIL-53(Al) for nano filtration †, RSC
558 Adv. 5 (2015) 73068–73076. doi:10.1039/C5RA10259F.

559 [29] S. Basu, A. Cano-odena, I.F.J. Vankelecom, Asymmetric
560 Matrimid®/[Cu3(BTC)2] mixed-matrix membranes for gas separations, J.
561 Membr. Sci. 362 (2010) 478–487. doi:10.1016/j.memsci.2010.07.005.

562 [30] L.C. Tomé, D. Mecerreyes, C.S.R. Freire, L.P.N. Rebelo, I.M. Marrucho,
563 Pyrrolidinium-based polymeric ionic liquid materials: New perspectives for
564 CO2 separation membranes, J. Membr. Sci. 428 (2013) 260–266.
565 doi:10.1016/j.memsci.2012.10.044.

566 [31] R. Abedini, M. Omidkhah, F. Dorosti, Hydrogen separation and
567 purification with poly (4-methyl-1-pentyne)/MIL 53 mixed matrix
568 membrane based on reverse selectivity, Int. J. Hydrog. Energy. 39 (2014)
569 7897–7909. doi:10.1016/j.ijhydene.2014.03.027.

[32] S. Shahid, K. Nijmeijer, Performance and plasticization behavior of polymer – MOF membranes for gas separation at elevated pressures, J. Membr. Sci. 470 (2014) 166–177. doi:10.1016/j.memsci.2014.07.034.

[33] Z. Liang, M. Marshall, A.L. Chaffee, CO2 adsorption-based separation by metal organic framework (Cu-BTC) versus zeolite (13X), Energy Fuels. 23 (2009) 2785–2789. doi:10.1021/ef800938e.

[34] M.J.C. Ordoñez, K.J. Balkus, J.P. Ferraris, I.H. Musselman, Molecular sieving realized with ZIF-8/Matrimid® mixed-matrix membranes, J. Membr. Sci. 361 (2010) 28–37. doi:10.1016/j.memsci.2010.06.017.

[35] E.L. Cussler, Fundamentals of Mass Transfer, Third edit, Cambridge University Press, New York, 2009. doi:10.1017/CBO9780511805134.010.

[36] X.Y. Chen, H. Vinh-Thang, D. Rodrigue, S. Kaliaguine, Amine-functionalized MIL-53 metal-organic framework in polyimide mixed matrix membranes for CO2/CH4separation, Ind. Eng. Chem. Res. 51 (2012) 6895–6906. doi:10.1021/ie3004336.

[37] Z. Dong, Z. Mi, W. Shi, H. Jiang, Y. Zheng, K. Yang, High pressure effects on hydrate Cu-BTC investigated by vibrational spectroscopy and synchrotron X-ray diffraction, RSC Adv. 7 (2017) 55504–55512. doi:10.1039/C7RA11843K.

[38] C. Zhang, Y. Dai, J.R. Johnson, O. Karvan, W.J. Koros, High performance ZIF-8/6FDA-DAM mixed matrix membrane for propylene/propane separations, J. Membr. Sci. 389 (2012) 34–42. doi:10.1016/j.memsci.2011.10.003.

[39] H. Li, L. Tuo, K. Yang, H.K. Jeong, Y. Dai, G. He, W. Zhao, Simultaneous enhancement of mechanical properties and CO2selectivity of ZIF-8 mixed matrix membranes: Interfacial toughening effect of ionic liquid, J. Membr. Sci. 511 (2016) 130–142. doi:10.1016/j.memsci.2016.03.050.

[40] A.R. Nabais, R.P.P.L. Ribeiro, J.P.B. Mota, V.D. Alves, I.A.A.C. Esteves, L.A. Neves, CO2/N2 Gas Separation using Fe(BTC)-based Mixed Matrix Membranes: A view on the adsorptive and filler properties of Metal-Organic Frameworks, Sep. Purif. Technol. 202 (2018) 174–184. doi:10.1016/j.seppur.2018.03.028.

[41] B. Monteiro, A.R. Nabais, F.A. Almeida Paz, L. Cabrita, L.C. Branco, I.M. Marrucho, L.A. Neves, C.C.L. Pereira, Membranes with a low loading of Metal–Organic Framework-Supported Ionic Liquids for CO2/N2separation in CO2capture, Energy Technol. 5 (2017) 2158–2162. doi:10.1002/ente.201700228.

[42] M. Sadeghi, M.A. Semsarzadeh, H. Moadel, Enhancement of the gas separation properties of polybenzimidazole (PBI) membrane by incorporation of silica nano particles, J. Membr. Sci. 331 (2009) 21–30. doi:10.1016/j.memsci.2008.12.073.

[43] V. Giel, M. Perchacz, J. Kredatusová, Z. Pientka, Gas Transport Properties of Polybenzimidazole and Poly(Phenylene Oxide) Mixed Matrix Membranes Incorporated with PDA-Functionalised Titanate Nanotubes, Nanoscale Res. Lett. 12 (2017) 3–17. doi:10.1186/s11671-016-1613-4.

[44] A.L. Khan, A. Cano-Odena, B. Gutierrez, C. Minguillon, I.F.J. Vankelecom, Hydrogen separation and purification using polysulfone

617 acrylate-zeolite mixed matrix membranes, J. Membr. Sci. 350 (2010)
618 340–346. doi:10.1016/j.memsci.2010.01.009.

619 [45] E. V. Perez, K.J. Balkus, J.P. Ferraris, I.H. Musselman, Mixed-matrix
620 membranes containing MOF-5 for gas separations, J. Membr. Sci. 328
621 (2009) 165–173. doi:10.1016/j.memsci.2008.12.006.

622 [46] J.R. Li, Y. Ma, M.C. McCarthy, J. Sculley, J. Yu, H.K. Jeong, P.B.
623 Balbuena, H.C. Zhou, Carbon dioxide capture-related gas adsorption and
624 separation in metal-organic frameworks, Coord.Chem. Rev. 255 (2011)
625 1791–1823. doi:10.1016/j.ccr.2011.02.012.

626 [47] P.S. Goh, A.F. Ismail, S.M. Sanip, B.C. Ng, M. Aziz, Recent advances of
627 inorganic fillers in mixed matrix membrane for gas separation, Sep. Purif.
628 Technol. 81 (2011) 243–264. doi:10.1016/j.seppur.2011.07.042.

629 [48] B.W. Rowe, L.M. Robeson, B.D. Freeman, D.R. Paul, Influence of
630 temperature on the upper bound: Theoretical considerations and
631 comparison with experimental results, J. Membr. Sci. 360 (2010) 58–69.
632 doi:10.1016/j.memsci.2010.04.047.

633